ADVANCED OPTICAL MATERIALS
www.advopticalmat.de

New UV-A Photodetector Based on Individual Potassium Niobate Nanowires with High Performance

*Hui Liu, Zhiming Zhang, Linfeng Hu, Nan Gao, Liwen Sang, Meiyong Liao, Renzhi Ma, Fangfang Xu, and Xiaosheng Fang**

A new UV-A photodetector based on $K_2Nb_8O_{21}$ nanowire is successfully fabricated for the first time. The potassium niobate is synthesized using a facile molten method. The $K_2Nb_8O_{21}$ nanowire photodetectors exhibit an excellent sensitivity and wavelength selectivity with respect to UV-A light. Furthermore, the photodetectors show great advantages in response time compared with other sensors based on single-oxide semiconductor nanostructures, and, especially, the responsivity is much better than that of single ZnS nanobelt photodetectors. The mechanism of conductivity is explained from the viewpoints of field emission and thermionic field emission for the change of light intensities.

1. Introduction

Over the past decades, great progress has been made in developing various types of nanodevice, such as solar cells,[1–3] field-effect transistors (FETs),[4–6] biological and chemical sensors,[7,8] energy storage devices,[9] photodetectors,[10–16] etc. Among these nanodevices, UV photodetectors have a wide range of applications in industry, including optical imaging, environmental monitoring, and air and water sterilization, as well as flame sensing and early rocket plume detection.[17] UV light is highly ionising electromagnetic radiation, invisible to the naked eye, with a wavelength in the range of 10–400 nm, which activates many chemical processes. It is typically divided into three spectral regions: UV-A (400–320 nm), UV-B (320–280 nm), and UV-C (280–200 nm), according to its effects on the biosphere. The far UV (200–10 nm), also commonly referred to as vacuum ultraviolet, however, is absorbed by oxygen and only exists in the vacuum condition.[18–20] UV light with wavelengths shorter than 320 nm (UV-C and UV-B) is mostly absorbed by the stratospheric ozone layer, but UV-A (320–400 nm) light can reach the Earth's surface. It is believed that overexposure to UV-A may lead to premature aging and even skin cancer, in spite of the use of sunscreen that can absorb or reflect some of the UV radiation on the skin against sunburn.[19,20] Although a variety of photodetectors based on low-dimensional nanostructures have been reported of different wavelength ranges, the research on UV-A irradiation detection is rather limited. One-dimensional (1D) semiconductor nanostructures are considered as excellent building blocks for constructing novel nanodevices due to their unique physical and chemical properties. As a matter of fact, UV-A photodetectors based on 1D semiconductor nanomaterials, such as ZnS,[21] ZnO,[22–25] SnO_2,[26,27] and Nb_2O_5,[28] have already been probed. Nevertheless, ZnS suffers from low photocurrent, while the sensitivities of the photodetectors made from the oxide semiconductors, as for ZnO, SnO_2, and Nb_2O_5, are retarded by either a high dark current or a low response speed. Thus, it is of highly importance to further develop UV-A light sensitive photodetectors with high performance.

Alkaline niobates exhibit various interesting properties, including nonlinear optical response,[29–31] ionic conductivity,[32] ferroelectricity,[33] piezoelectricity,[34] and photocatalytic activity.[35,36] Potassium niobate, with the composition $K_2Nb_8O_{21}$, is known for its good dielectric property and effective photocatalytic activity.[37,38] Also, it can be used as an intermediate for the synthesis of $NaNbO_3$ nanorods and $CaNb_2O_6$ nanorods through an ion-exchange approach.[39] $K_2Nb_8O_{21}$ occurs as an orthorhombic form and its bandgap, estimated from its UV–vis spectrum, is approximately 3.1 eV (ca. 400 nm).[36,37] Therefore, $K_2Nb_8O_{21}$ has great potential for UV-A light detection. Herein, we synthesized $K_2Nb_8O_{21}$ nanowires using a facile molten method, and, based on the as-prepared nanowires, fabricated UV-A light sensors. Compared with the aforementioned UV-A photodetectors, the presently studied $K_2Nb_8O_{21}$ nanowire photodetectors displayed superior response speed, selectivity, and sensitivity.

H. Liu, Z. M. Zhang, Prof. L. F. Hu, Dr. N. Gao, Prof. X. S. Fang
Department of Materials Science Fudan University
Shanghai 200433, PR China
E-mail: xshfang@fudan.edu.cn
Dr. L. W. Sang, Prof. M. Y. Liao, Prof. R. Z. Ma
National Institute for Materials Science (NIMS)
Namiki 1–1, Tsukuba
Ibaraki 305–0044, Japan
Prof. F. F. Xu
State Key Laboratory of High Performance Ceramics and Superfine Microstructures Shanghai Institute of Ceramics Chinese Academy of Sciences
Shanghai 200050, PR China

DOI: 10.1002/adom.201400176

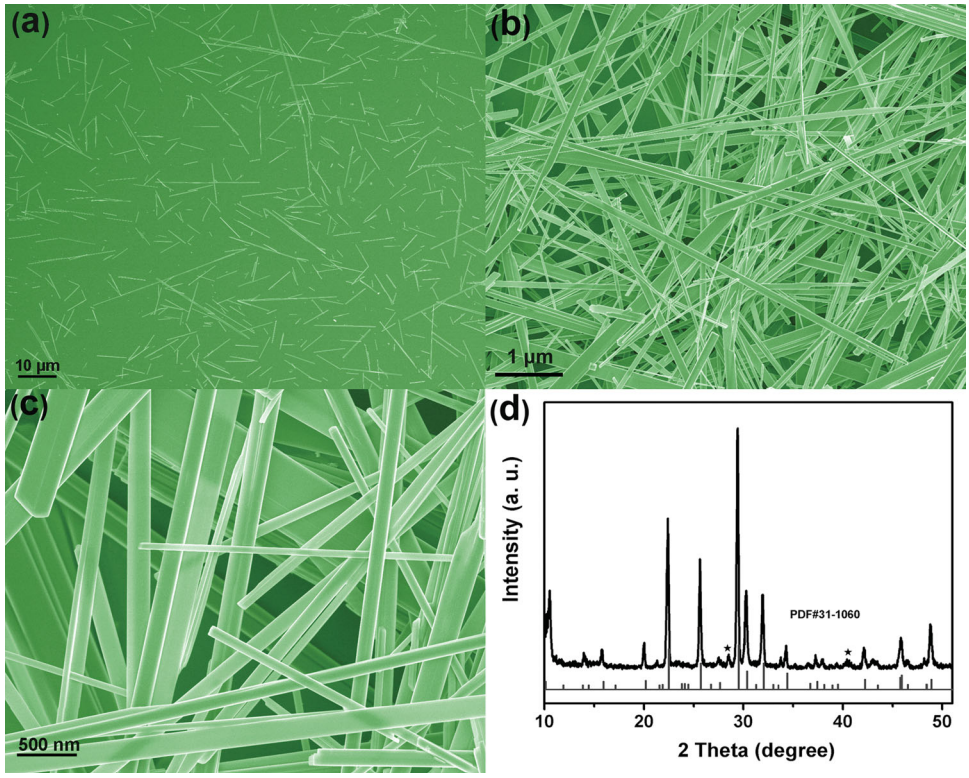

Figure 1. a–c) Low- and high-magnification scanning electron microscopy (SEM) images of the as-obtained $K_2Nb_8O_{21}$ nanowires. d) XRD patterns of $K_2Nb_8O_{21}$, with reference to standard potassium niobate.

2. Results and Discussion

From **Figure 1**a–c, it is noticed that the as-synthesized sample was composed of many freestanding nanowires at a significant percentage (ca. 20% to 40%) of the yield, which were interspersed with a number of large microwires and nanobelts. Statistics indicates that the main distribution width and length of the $K_2Nb_8O_{21}$ nanowires are 130 nm and 20 μm, respectively, with a yield of ca. 30%. The X-ray diffraction (XRD) pattern of the nanowires is shown in Figure 1d. The diffraction peaks are identified as those of $K_2Nb_8O_{21}$ according to JCPDS 31–1060, whereas the two diffraction peaks with asterisks are ascribed to KNb_3O_8 impurities.[37,38] Although single-crystal $K_2Nb_8O_{21}$ was successfully synthesized decades ago,[40] the crystal structure and lattice parameters were not well understood because of the large number of microsized domains lying perpendicular to each other in the single crystals. Teng and co-workers examined the structures using high-resolution transmission electron microscopy (HR-TEM) and electron diffraction techniques, and drew the conclusion that $K_2Nb_8O_{21}$ are of pertinence to the orthorhombic system, with lattice parameters a = 37.5 Å, b = 12.5 Å, and c = 3.96 Å, and the $P2_12_12$ space group.[41] X-ray photoelectron spectroscopy (XPS) (**Figure 2**) confirmed that only K, Nb and O were present in the sample. The single peak at 205.7 eV is assigned to Nb 3d 5/2, indicating that the $K_2Nb_8O_{21}$ nanowires just contained Nb^{5+} on the surface.

HR-TEM and selected area electron diffraction (SAED) were conducted to further confirm the morphology and structure of individual nanowires. **Figure 3**a shows a low-magnification image of a typical nanowire, suggesting that the obtained products had wire-like morphology. The 0.396 and 0.936 nm spacings of the lattice fringes in Figure 3b match well with the (001) and (400) planes, in accordance with the Miller index deduced from the lattice parameters and space group. The inset SAED image shows very sharp diffraction spots, suggesting the single-crystal instinct of the nanowire. The (001) plane is oriented perpendicular to the growth axis of the nanowire, implying the growth direction is along the [001] axis. SAED patterns along another two zone axis of the nanowires are given in Figure 3c and 3d. In order to further confirm the chemical composition and elemental distribution, X-ray energy dispersive spectroscopy (EDS) was performed on a single nanowire, as shown in **Figure 4**. It is obvious that the three elements of K, Nb, and O are homogeneously distributed within the nanowire, and this is further supported by the uniform distribution of these elements along the red line of the high-angle annular dark-field (HAADF) image in Figure 4a.

Figure 5a shows typical current–voltage (I–V) curves measured with respect to the nanowire-based photodetector device by a two-probe method in room-temperature air. The inset in Figure 5a is an SEM image of the device. The Ti/Au parallel electrodes (100 nm/100 nm) were deposited on a $K_2Nb_8O_{21}$ nanowire with diameter of ca. 150 nm and length of ca. 40 μm. When the wavelength of the light source was longer than 400 nm, there was almost no response from the device, and the photocurrent and the dark current were overlapped with each other. In contrast, under illumination wavelengths shorter than 400 nm, the photocurrent increased drastically,

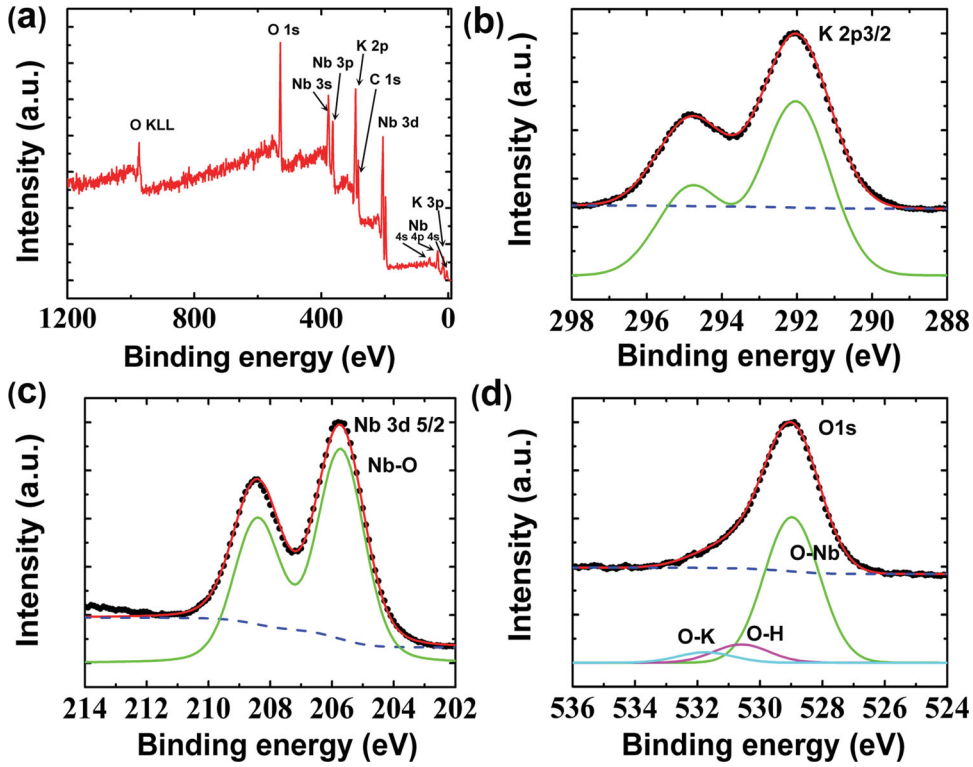

Figure 2. a) XPS survey scan of $K_2Nb_8O_{21}$ nanowires (upper left). The residual carbon signal around 286 eV always exists in the XPS spectra. b–d) High resolution XPS spectra for K (upper right), Nb (lower left), and O (lower right).

as for the wavelength of 320 nm (126 μW cm^{-2}), to 12.5 pA, more than one order-of-magnitude larger. Further decreasing the wavelength of the light source resulted in a decay in photocurrent, to 5.57 pA at 300 nm (75 μW cm^{-2}) and 4.65 pA at 250 nm (11.6 μW cm^{-2}), mainly ascribed to the decreasing light intensity.

The spectral responsivity (R_λ) and external quantum efficiency (*EQE*) are two important parameters to determine the sensitivity of an optoelectronic device,[27,28] and can be calculated using the following equations, respectively:

$$R_\lambda = \frac{\Delta I}{PS} \tag{1}$$

$$EQE = \frac{hc}{e\lambda} R_\lambda \tag{2}$$

where ΔI is the difference between the photocurrent and the dark current, P is the light power, S is the irradiated area on the nanowire, h is Planck's constant, c is the velocity of light, e is the electronic charge, and λ is the exciting wavelength. The calculated R_λ and *EQE* of the present nanowire device were as high as 2.53 A/W and 982%, respectively, at 320 nm under an applied voltage of 5 V. Besides, most *I–V* curves show nonlinear behavior, which should be related to the Schottky blocking at the metal/semiconductor contacts. When the light intensities were changed, the photocurrent exhibited a more obvious dependence on the applied voltage, as shown in Figure 5b. A thermionic-field emission (TFE) mechanism or a field emission (FE) mechanism can be used to describe the changes in photocurrent at interface contacts.[42,43] It is demonstrated in Figure 5b that, at a low applied voltage, the current follows an approximately exponential increase, as expected from the relationship below:

$$J_{\mathrm{TFE}} = J_s \exp\left(\frac{V}{E_0}\right), \text{where } E_0 = E_{00} \coth\left(\frac{E_{00}}{kT}\right) \tag{3}$$

where J_s is the saturation current density, V is the applied voltage, k is the Boltzmann constant, T is temperature, and E_{00} reflects the tunnelling probability.[43,44] The dependence of the photocurrent upon voltage, when it is high, can be understood as a Fowler-Nordheim (FE) process, where $J_{\mathrm{FN}} \propto V^2 \exp(\frac{b}{V} + a)$.[44,45] The photocurrent is well described using the above transport mechanisms. When the light intensity is 128 μW cm^{-2}, for example, it is found that the *I–V* curve is well fitted with TFE mechanism at low voltages (from 0.30 to 4.3 V) and the mechanism of FE at high voltages (from 4.3 to 5 V), where a and b are –17.9 and –47.2, respectively. In addition, the photocurrent is exponentially proportional to light intensity, as shown in Figure 5c, the photoresponse is fitted with a power law, $I \propto P^{0.44}$, and the non-unity exponent indicates a complex process of electron–hole generation, trapping, and recombination within the semiconductor.[23,24] Moreover, the *EQE* exhibits distinct behavior at different voltages, as shown in Figure 5d, suggesting the TFE and FE mechanisms have different effects on the transport processes of charge carriers (electron and hole)

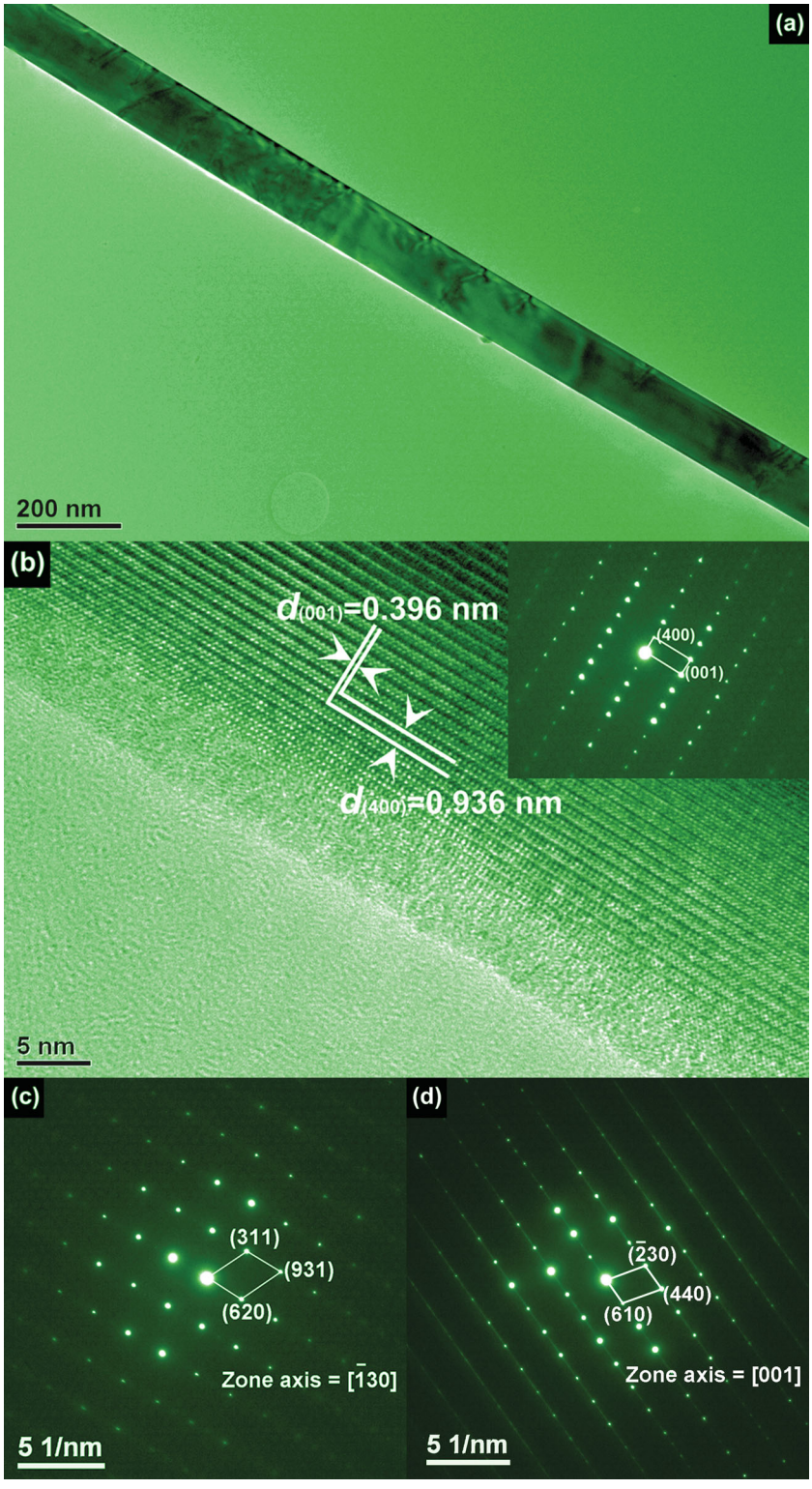

Figure 3. a) TEM image, and, b) HR-TEM image of a typical nanowire. The inset of b is the corresponding SAED pattern. c–d) SAED patterns along another two zone axis of the nanowires.

at interface contacts. At the low voltage of 2 V, the *EQE* almost remains unchanged with the increasing of light intensity. This is because the voltage is not high enough for the photo-induced charge carriers to tunnel to the electrode. In this case, the TFE mechanism at the interface plays a less important role and the conducting process is only decided by the semiconductor itself. On the other hand, the *EQE* presents a declining trend at the high voltage of 5 V. One possible reason is that more charge carriers are injected and accumulated at the interface contacts because of FE at high voltage, and some of them cannot rapidly tunnel to the electrode to contribute the photocurrent, thus, leading to the decrease of *EQE*.[46]

In addition to the high sensitivity, the nanowire photodetector also shows prominent wavelength selectivity. **Figure 6**a represents the spectral response for the photodetector at a bias of 5 V with the wavelength changing from 630 to 300 nm. It is noticed that a discrimination ratio (between 300 nm UV light and 500 nm visible light) of about more than 3 orders is obvious. The high sensitivity and spectral selectivity suggest that the present nanowire photodetector is intrinsically "visible-light-blind". The band gap (E_g) of $K_2Nb_8O_{21}$ speculated from the spectral response is about 3.1 eV (ca. 400 nm), in accordance with the UV-vis evaluation (inset of Figure 6a). Apart from sensitivity and selectivity, the response speed is another key factor to evaluate the sensor performances. Figure 6b represents the reversible time response of this photodetector between low- and high-conductance states, upon 320 nm light illumination at a applied voltage of 5 V. It can be observed that the current changes immediately when the transition between light-on and light-off takes place, indicating that the rise/decay time (defined as the time required for the photocurrent to increase from 10% to 90%/drop from 90% to 10%) is less than 0.3 s (limitation of the measurement system). The reversible periodic changes between the photocurrent and the dark current upon turning on/off of the laser irradiation reveal that the results generated of the present photodetectors are well reproducible and stable.

It is generally accepted that oxygen chemisorption plays a fairly key role in regulating the photoconductive process in oxide semiconductors, whereas this phenomenon is more conspicuous in nanodevices due to their large surface-to-volume ratios.[23,24] A similar mechanism is believed applicable to the present nanowire system; as potassium niobate is composed of the NbO_6 building blocks, oxygen chemisorption may also play an influential role in photoconductivity. Taking this into account, we investigate the *I–V* characteristics of the

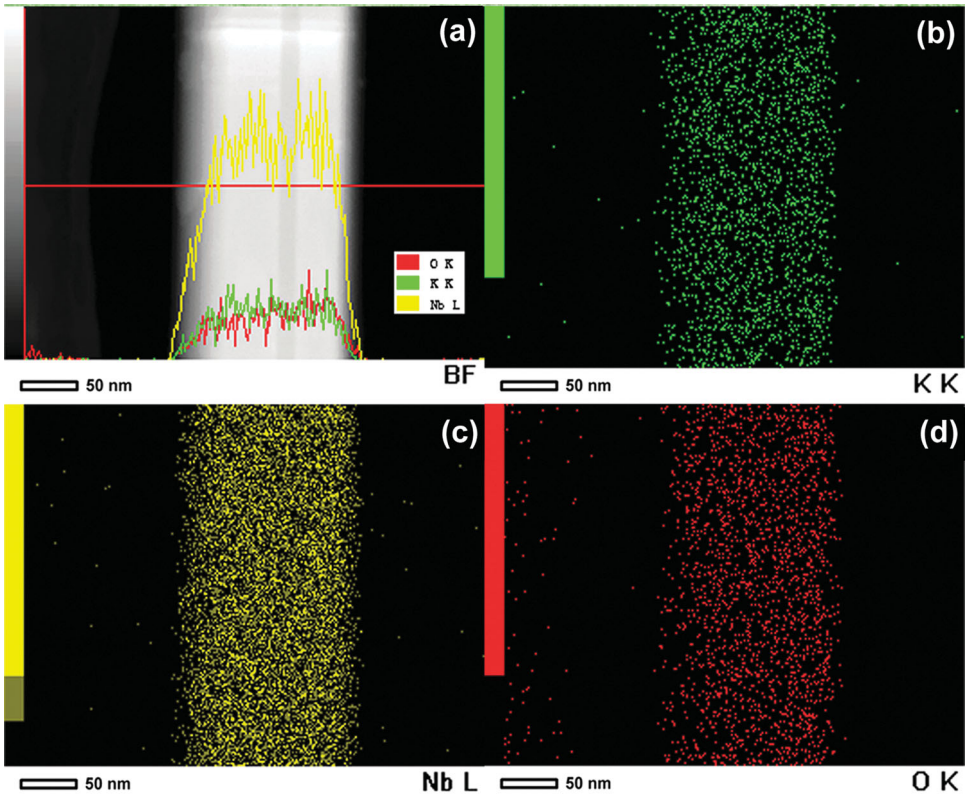

Figure 4. a) HADDF Scanning TEM image and EDS line-scan along the red line. b–d) Corresponding EDS mapping for K (green), Nb (yellow), and O (red), respectively, of the nanowire in a.

present photodetector under different atmospheres. As shown in Figure 6c, the current indeed shows an increase when the atmosphere is switched from ambient to vacuum (100 Pa) conditions. The dark current and the photo-induced current are 1.2 and 13.5 pA, respectively, under ambient conditions, and both increase up to 3.4 and 32.2 pA at 100 Pa. At ambient conditions, oxygen molecules are absorbed on the nanowire, and capture free electrons from the nanowire, forming negative charged ions [O_2 (g) + $e^- \rightarrow O_2^-$ (ad)]. This creates a depletion region near the nanowire surface which decreases the carrier lifetime, and results in a high resistance or low conductivity in the dark state. When exposed to UV light with energy greater than the bandgap, the nanowire will generate electron–hole pairs, and the holes migrate to the surface and combine with negatively charged oxygen through the reaction [$h^+ + O_2^-$ (ad) $\rightarrow O_2$ (g)]. Thus, the photo-induced electrons under the driving of external electric field can lead to an apparent enhancement of photocurrent in air. In vacuum, however, the dark current increases by ca. 2 times, in comparison to the value obtained by the measurement in air, which is in agreement with the reports by other groups.[47,49,50] This increase of dark current is due to the increase of the carrier lifetime caused by the desorption of oxygen adsorbed on the nanowire surface under vacuum conditions. On the other hand, the photocurrent under 100 Pa is 2.4 times larger than that under atmospheric pressure, which is consistent with previous reports of an enhancement of both photocurrent and photoluminescence in vacuum.[15,28,51] Since the diameter of the nanowire is larger than 100 nm, the nanowire cannot be entirely depleted, which will result in the bending of the surface band at the nanowire sidewall facets. It is easier for oxygen to be photodesorbed from the surface of the nanowire surface under both vacuum and UV illumination, hence bringing up a larger concentration of free electrons and prolonging the photocurrent decay times. Consequently, a slightly increased dark current and an obviously enhanced photocurrent are resulted in vacuum. Furthermore, the current–time responses measured in alternating conditions of vacuum and air are also illustrated in Figure 6d; the substantial changes in vacuum may be due to the fluctuation of low pressure. It is noticed that both types of currents are relatively stable with fast responses. As summarized in **Table 1**, the performances of the $K_2Nb_8O_{21}$ nanowire photodetector for UV-A detection show great advantages in response time compared with other sensors based on single-oxide semiconductor nanostructures, and, especially, the responsivity is much better than that of single-nanobelt (ZnS and ZnSe) photodetectors. It should be noted that, since the UV light source is the third harmonic of a Nd:YAG laser, the ZnO nanowires observed by Kind et al.[23] show faster response time compared with other two ZnO nanowire samples.

3. Conclusion

Photodetectors based on individual $K_2Nb_8O_{21}$ nanowires were fabricated for the first time. The potassium niobate was synthesized using a facile molten method. The single-nanowire

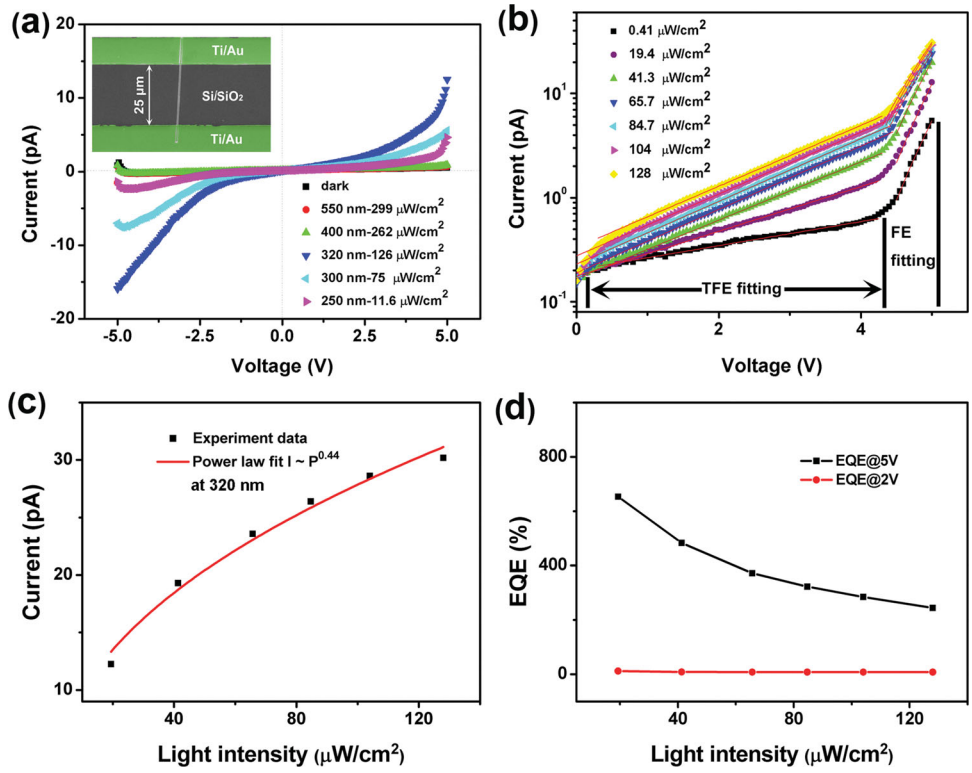

Figure 5. a) *I–V* curves of the single-nanowire photodetector illuminated with 250–550 nm light and under the dark condition, respectively, at 5 V. Inset is the SEM image of the device. b) *I–V* characteristics of the nanowire photodetector under illumination of 320 nm light while the intensities of incident light are changed. The solid lines fit TFE and FE tunneling mechanisms at different light intensities. c) Variation of photocurrent at 5 V. d) *EQE* with the light intensity at 320 nm for the present photodetector at 2 and 5 V, respectively.

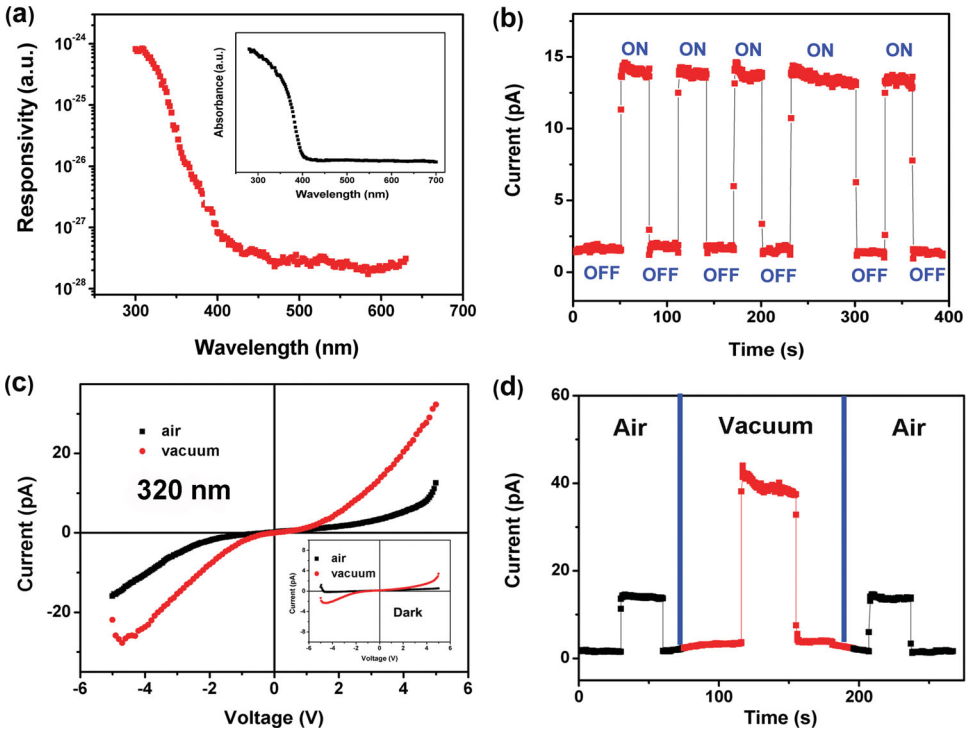

Figure 6. a) Spectral response of the nanowire photodetector against wavelength ranged from 630 to 300 nm measured at a bias of 5 V. The inset is the UV-vis absorption spectrum. b) Current–time response of the $K_2Nb_8O_{21}$ nanowire photodetector illuminated with 320 nm light measured using a mechanical chopping method at 5V. c) *I–V* characteristics upon 320 nm illumination in air and vacuum, respectively. The inset shows the *I–V* curves in the dark. d) Current–time responses of the nanowire photodetector under air–vacuum–air conditions.

Table 1. Comparison of the characteristic parameters for $K_2Nb_8O_{21}$ nanowire photodetectors and other photodetectors.

Photodetector	Light of detection	Bias	Dark Current	Photocurrent	R_λ	EQE/Gain	Rise time	Decay time	Reference
ZnO nanowire	350 nm; 1.3 mW cm^{-2}	1.0 V	0.13 pA	0.13 nA	—	—	40 s	300 s	[22]
ZnO nanowire	365 nm; Nd:YAG laser, 0.3 mW cm^{-2}	5.0 V	ca. 1 pA	ca. 250 nA	—	—	<1 s	<1 s	[23]
ZnO nanowire	390 nm; 40 mW cm^{-2}	5.0 V	1–10 nA	100 μA	—	2×10^8	23 s	33 s	[24]
An array of ZnO nanowires	Ti:sapphire laser system; ultrafast laser pulses; 0.3 μJ pulse^{-1}	1.0 V	ca. 1 μA	ca. 20 μA	—	—	ca. 20 ns	ca. 20 ns	[24]
ZnO nanowire	355 nm; 6 mW cm^{-2}	0.1 mV	4.5 μA	—	0.0075	0.04	500 ns	6.7 μs	[25]
Pulsed laser					A/W at –5 V				
SnO_2 nanowire	325 nm; 10 mW cm^{-2}	1.0 V	19.4 nA	2.1 μA	—	—	>40 s	>40 s	[26]
SnO_2 nanowire	320 nm; 0.91 mW cm^{-2}	0.1 V	40 nA	200 nA	—	1.32×10^7	>40 s	>100 s	[27a]
Nb_2O_5 nanobelt	320 nm; 0.91 mW cm^{-2}	1.0 V	15.5 pA	51.3 pA	15.2 A/W at 1 V	60.7	—	—	[28a]
ZnS nanobelt	320 nm; 0.91 mW cm^{-2}	5.0 V	<0.1 pA	ca. 0.6 pA	—	—	< 0.3 s	< 0.3 s	[21]
GaN nanowire	244 nm; 0.2 mW cm^{-2}	3.0 V	—	—	—	10^5–10^8	—	4–10 ms	[47]
ZnSe nanobelt	400 nm; 2.02 mW cm^{-2}	30 V	<0.01 pA	ca. 1.7 pA	0.12 A/W at 30 V	0.372	<0.3 s	<0.3 s	[48]
$K_2Nb_8O_{21}$ nanowire	320 nm; 0.12 mW cm^{-2}	5.0 V	1.2 pA	13.5 pA	2.53 A/W at 5 V	9.82	<0.3 s	<0.3 s	This work

photodetectors show a remarkable sensitivity and wavelength selectivity with respect to UV-A light. Furthermore, the photodetectors exhibited rapid responsive, high discrimination ratio, robust stability, and a strong dependence of photocurrent on light intensity. The mechanism of conductivity was explained from the viewpoints of field emission and thermionic-field emission for the change of light intensities. These results satisfactorily justify the potential of potassium niobate nanowires for high-performance UV-A photodetectors.

4. Experimental Section

Synthesis of the potassium niobate was conducted in a conventional horizontal furnace with a 5 cm inner-diameter quartz tube. A mixture of raw materials, typically 0.3 g of Nb_2O_5 (Aladdin, 99.99%) powder in 1.6 g of molten KCl (Sinopharm, AR), was transferred to a crucible (size: 7 cm × 2 cm × 2 cm) and covered with another crucible to keep KCl from evaporation. The crucibles were then mounted to the tube, at 900 °C for 3 h, in such a way that the heat was concentrated at the center of the crucible. The obtained white products were washed using hot deionized water several times to remove residual salt. The phase of as-obtained $K_2Nb_8O_{21}$ nanowires was identified by a Rigaku D/max-rB x-ray diffractometer using Cu Kα radiation (λ = 0.15406 nm) in the 2θ range from 10° to 60°. The morphology of the products characterization was carried out by using field-emission scanning electron microscopy (FESEM) (JEOL JSM-6701F) and transmission electron microscope (TEM) (JEOL JEM-2100F) equipped with an X-ray energy dispersive spectrometer (EDS). The UV-vis adsorption spectra were scanned with a Hitachi U-4100 spectrophotometer with the wavelength from 700 to 200 nm. The XPS measurements were performed by a monochromated Al Kα X-ray source ($h\nu$ = 1486.6 eV) with vacuum pressure of 1.0×10^{-9} Torr.

For the fabrication of single-nanowire photodetectors, the $K_2Nb_8O_{21}$ nanowires, in the first place, were dispersed in acetone and deposited drop-wise on a Si substrate with a 300 nm SiO_2 top layer. The Ti/Au (100/100 nm) electrodes were then patterned on the top of the nanowires through photolithography, magnetron sputtering, and lift-off process. The current–voltage characteristics of the $K_2Nb_8O_{21}$ nanowire photodetectors were measured using an Advantest Picoammeter R8340A and a DC voltage source R6144. The spectral response for different wavelengths was recorded using a xenon lamp (500 W).

Acknowledgements

The authors thank Dr. J. Yan and Dr. J. W. Liu from Hefei University of Technology and the National Institute for Materials Science (NIMS) for the discussions of XRD indices and XPS measurements, respectively. This work was supported by the Science and Technology Commission of Shanghai Municipality (13NM1400300), the Project of Short-Term International Visiting for PhD Candidates at Fudan University (2013), the Shanghai Shu Guang Project (12SG01), the Shanghai Pujiang Program (12PJ1400300), the National Natural Science Foundation of China (grant nos. 91123006 and 51372040), the Innovation Program of Shanghai Municipal Education Commission (14ZZ003), and the Programs for Professor of Special Appointment (Eastern Scholar) at Shanghai Institutions of Higher Learning and for New Century Excellent Talents in University (NCET-11–0102).

Received: April 21, 2014
Revised: May 21, 2014
Published online: June 27, 2014

[1] B. Z. Tian, X. L. Zheng, T. J. Kempa, Y. Fang, N. F. Yu, G. H. Yu, J. L. Huang, C. M. Lieber, *Nature* **2007**, *449*, 885.
[2] J. S. Luo, S. K. Karutruri, L. J. Liu, L. T. Su, A. L. Y. Tok, H. J. Fan, *Sci. Rep.* **2012**, *2*, 451.
[3] M. Chen, C. Y. Ye, S. X. Zhou, L. M. Wu, *Adv. Mater.* **2013**, *25*, 5343.
[4] B. Z. Tian, J. Liu, T. Dvir, L. H. Jin, J. H. Tsui, Q. Qing, Z. G. Suo, R. Langer, D. S. Kohane, C. M. Lieber, *Nat. Mater.* **2012**, *11*, 986.
[5] Y. L. Zhang, L. Guo, H. Xia, Q. D. Chen, J. Feng, H. B. Sun, *Adv. Opt. Mater.* **2014**, *2*, 10.
[6] R. Graham, D. Yu, *Nano Lett.* **2012**, *12*, 4360.
[7] X. M. Zou, J. L. Wang, X. Q. Liu, C. L. Wang, Y. Jiang, Y. Wang, X. H. Xiao, J. C. Ho, J. C. Li, C. Z. Jiang, Y. Fang, W. Liu, L. Liao, *Nano Lett.* **2013**, *13*, 3287.

[8] X. F. Pan, X. Liu, A. Bermark, Z. Y. Fan, *ACS Nano* **2013**, *7*, 9318.
[9] J. Jiang, Y. Y. Li, J. P. Liu, X. T. Huang, C. Z. Yuan, X. W. Lou, *Adv. Mater.* **2012**, *24*, 5166.
[10] L. Li, P. C. Wu, X. S. Fang, T. Y. Zhai, L. Dai, M. Y. Liao, Y. Koide, H. Q. Wang, Y. Bando, D. Golberg, *Adv. Mater.* **2010**, *22*, 3161.
[11] F. W. Guo, Z. G. Xiao, J. S. Huang, *Adv. Opt. Mater.* **2013**, *1*, 289.
[12] W. Tian, T. Y. Zhai, C. Zhang, S. L. Li, X. Wang, F. Liu, D. Q. Liu, X. K. Cai, K. Tsukagoshi, D. Golberg, Y. Bando, *Adv. Mater.* **2013**, *25*, 4625.
[13] L. Peng, L. F. Hu, X. S. Fang, *Adv. Mater.* **2013**, *25*, 5321.
[14] H. Q. Wang, A. Pyatenko, N. Koshizaki, H. Moehwald, D. Shchukin, *ACS Appl. Mater. Interfaces* **2014**, *6*, 1141.
[15] W. Tian, C. Zhang, T. Y. Zhai, S. L. Li, X. Wang, J. W. Liu, X. Jie, D. Q. Liu, M. Y. Liao, Y. Koide, D. Golberg, Y. Bando, *Adv. Mater.* **2014**, *26*, 3088.
[16] M. Y. Chen, H. Yu, S. V. Kershaw, H. H. Xu, S. Gupta, F. Hetsch, A. L. Rogach, N. Zhao, *Adv. Funct. Mater.* **2014**, *24*, 53.
[17] G. Konstantatos, E. H. Sargent, *Nat. Nanotechnol.* **2010**, *5*, 391.
[18] L. W. Sang, M. L. Liao, M. Sumiya, *Sensors* **2013**, *13*, 10482.
[19] E. Monroy, F. Omnes, F. Calle, *Semicond. Sci. Technol.* **2003**, *18*, R33.
[20] P. E. Hockberger, *Photochem. Photobiol.* **2002**, *76*, 561.
[21] X. S. Fang, Y. Bando, M. Y. Liao, U. K. Gautam, C. Y. Zhi, B. Dierre, B. D. Liu, T. Y. Zhai, T. Sekiguchi, Y. Koide, D. Golberg, *Adv. Mater.* **2009**, *21*, 2034.
[22] K. W. Liu, M. Sakurai, M. Y. Liao, M. Aono, *J. Phys. Chem. C* **2010**, *114*, 19835.
[23] H. Kind, H. Q. Yan, B. Messer, M. Law, P. D. Yang, *Adv. Mater.* **2002**, *2*, 158.
[24] C. Soci, A. Zhang, B. Xiang, S. A. Dayeh, D. P. R. Aplin, J. Park, X. Y. Bao, Y. H. Lo, D. Wang, *Nano Lett.* **2007**, *4*, 1003.
[25] S. M. Hatch, J. Briscoe, S. Dunn, *Adv. Mater.* **2013**, *25*, 867.
[26] C. H. Lin, R. S. Chen, T. T. Chen, H. Y. Chen, Y. F. Chen, K. H. Chen, L. C. Chen, *Appl. Phys. Lett.* **2008**, *93*, 112115.
[27] a) L. F. Hu, J. Yan, M. Y. Liao, L. M. Wu, X. S. Fang, *Small* **2011**, *7*, 1012; b) F. W. Guo, B. Yang, Y. B. Yuan, Z. G. Dong, Y. Bi, J. S. Huang, *Nat. Nanotechnol.* **2012**, *7*, 798; c) P. A. Hu, Z. Z. Wen, L. F. Wang, P. H. Tan, K. Xiao, *ACS Nano* **2012**, *7*, 5988.
[28] a) X. S. Fang, L. F. Hu, K. F. Huo, B. Gao, L. J. Zhao, M. Y. Liao, P. Chu, Y. Bando, D. Golberg, *Adv. Funct. Mater.* **2011**, *21*, 3907; b) L. Ma, W. Hu, Q. L. Zhang, P. Y. Ren, X. J. Zhuang, H. Zhou, J. Y. Xu, H. L. Li, Z. P. Shan, X. X. Wang, L. Liao, H. Q. Xu, A. L. Pan, *Nano Lett.* **2014**, *14*, 694.
[29] Y. Nakayama, P. J. Pauzauskie, A. Radenovic, R. M. Onorato, R. J. Saykally, J. Liphardt, P. Yang, *Nature* **2007**, *447*, 1098.
[30] S. Kim, J. Lee, J. Lee, S. W. Kim, M. H. Kim, S. Park, H. Chung, Y. I. Kim, W. Kim, *J. Am. Chem. Soc.* **2013**, *135*, 6.
[31] F. Dutto, C. Raillon, K. Schenk, A. Radenovic, *Nano Lett.* **2011**, *11*, 2517.
[32] R. Haugsrud, T. Norby, *Nat. Mater.* **2006**, *5*, 193.
[33] P. M. Rørvik, T. Grande, M. A. Einarsrud, *Adv. Mater.* **2011**, *23*, 4007.
[34] T. Y. Ke, H. A. Chen, H. S. Sheu, J. W. Yeh, H. N. Lin, C. Y. Lee, H. T. Chiu, *J. Phys. Chem. C* **2008**, *112*, 8827.
[35] P. Li, S. X. Ouyang, G. C. Xi, T. Kako, J. H. Ye, *J. Phys. Chem. C* **2012**, *116*, 7621.
[36] K. Saito, A. Kudo, *Inorg. Chem.* **2010**, *49*, 2017.
[37] C. Y. Xu, L. Zhen, J. T. Jiang, C. S. Lao, L. Yang, *Ceram. Int.* **2009**, *35*, 3021.
[38] K. Teshima, Y. Niina, K. Yubta, T. Nakazawa, T. Suzuki, T. Shishido, N. Ishizawa, S. Oishi, *Jpn. J. Appl. Phys.* **2008**, *47*, 629.
[39] C. Y. Xu, L. Zhen, R. S. Yang, Z. L. Wang, *J. Am. Chem. Soc.* **2007**, *129*, 15444.
[40] J. E. Guerchais, *Bull. Soc. Chim. Fr.* **1962**, *1*, 103.
[41] C. M. Teng, F. H. Li, D. Y. Yang, Q. Z. Wu, *J. Chin. Ceram. Soc.* **1986**, *4*, 484 (in Chinese).
[42] F. A. Padovani, R. Stratton, *Solid State Electron.* **1966**, *9*, 695.
[43] M. Y. Liao, X. Wang, T. Teraji, S. Koizumi, Y. Koide, *Phys. Rev. B* **2010**, *81*, 033304.
[44] L. W. Sang, M. Y. Liao, Y. Koide, M. Sumiya, *Appl. Phys. Lett.* **2011**, *99*, 031115.
[45] S. M. Sze, *Physics of Semiconductor Devices*, 2nd ed., Wiley, New York **1981**.
[46] V. D. Mihailetchi, J. Wildeman, P.W. M. Blom, *Phys. Rev. Lett.* **2005**, *94*, 126602.
[47] F. G. Posada, R. Songmuang, M. D. Hertog, E. Monroy, *Nano Lett.* **2012**, *12*, 172.
[48] X. S. Fang, S. L. Xiong, T. Y. Zhai, Y. Bando, M. Y. Liao, U. K. Gautam, Y. Koide, X. G. Zhang, Y. T. Qian, D. Golberg, *Adv. Mater.* **2009**, *21*, 5016.
[49] L. Rigutti, M. Tchernycheva, A. D. Bugallo, G. Jacopin, F. H. Julien, L. F. Zagonel, K. March, O. Stephan, M. Kociak, R. Songmuang, *Nano Lett.* **2010**, *10*, 2939.
[50] M. I. Hertog, F. G. Posada, R. Songmuang, J. L. Rouviere, T. Fournier, B. Fernandez, E. Monroy, *Nano Lett.* **2012**, *12*, sss5691.
[51] C. Pfüller, O. Brandt, F. Grosse, T. Flissikowski, C. Chèze, V. Consonni, L. Geelhaar, H. T. Grahn, H. Riechert, *Phys. Rev. B* **2010**, *82*, 045320.